Available online at www.sciencedirect.com
SCIENCE DIRECT®
Catalysis Today 107–108 (2005) 676–684
CATALYSIS TODAY
www.elsevier.com/locate/cattod

Dehydroaromatization of methane under non-oxidative conditions over bifunctional Mo/ITQ-2 catalysts

Agustín Martínez *, Ernest Peris, Germán Sastre

Instituto de Tecnología Química, UPV-CSIC, Avenida de los Naranjos s/n, 46022 Valencia, Spain

Available online 19 August 2005

Abstract

Bifunctional Mo/ITQ-2 catalysts have been used for the methane dehydroaromatization (MDA) reaction. The Si/Al ratio, and thus the Brønsted acidity, of the zeolite affected the conversion, the formation rate of aromatics, and the selectivity to the different products (CO, C_2, benzene, toluene, and naphthalene). Maximum activity and aromatics productivity were obtained for the zeolite with the lowest Si/Al ratio (Si/Al = 15) presenting the highest Brønsted acidity, while maximum benzene selectivity (~70%) occurred for the zeolite with Si/Al = 25. The selectivity to naphthalene increased with decreasing the Si/Al ratio, that is, with increasing the density of surface Brønsted acid sites. At comparable Si/Al ratio, Mo/MCM-22 was more active and selective to benzene than Mo/ITQ-2. Reduction of surface acidity in ITQ-2 by treatment with oxalic acid significantly reduced the formation of naphthalene, resulting in enhanced benzene selectivity (~75%). The acid-treated ITQ-2 was even more selective to benzene than the Mo/MCM-22 catalyst (~65%). Molecular dynamics simulations were performed at the MDA reaction temperature (973 K) to study the diffusion of naphthalene in the two independent pore systems of MCM-22. The theoretical results allowed explaining the differences in selectivity between the two zeolite structures and the effect of surface dealumination in ITQ-2.

Keywords: Methane dehydroaromatization; Bifunctional catalyst; Molybdenum; Delaminated zeolite; ITQ-2; Molecular dynamics simulation

1. Introduction

The direct conversion of methane to fuels and high-value chemicals still remains as one of the most important challenges in the field of heterogeneous catalysis [1]. Recently, Wang et al. [2] reported the direct conversion of methane under non-oxidative conditions into aromatics and hydrogen over a Mo/HZSM-5 catalyst. Since then, numerous studies have been devoted to the methane dehydroaromatization (MDA) process, with special emphasis into the optimization of the catalyst system and reaction conditions, the nature of active sites and reaction mechanisms, the interactions between the transition metal(s) and the zeolite support, and the role of carbonaceous deposits in the reaction [3].

A relevant aspect of the MDA reaction is the templating role of the zeolite micropores in determining the product selectivity, as recently reviewed by Shu and Ichikawa [4]. Indeed, although under typical MDA reaction conditions (973 K, 1 atm) naphthalene is the thermodynamically favored product, the Mo/HZSM-5 catalyst promoted the selective formation of benzene owing to the shape selectivity imposed by the 10 member-ring (10 MR) channels, which prevent the formation of the bulkier naphthalene molecule [5]. Recently, Mo/HMCM-22 catalysts have been found to produce higher yields of benzene and to exhibit better coke tolerance in comparison with Mo/HZSM-5 at comparable reaction conditions [6,7]. These properties were related to the particular topology of the MCM-22 zeolite. On one hand, the lower size of the pore entrances in MCM-22 (0.40 nm × 0.59 nm in the sinusoidal interlayer 10 MR system, and 0.40 nm × 0.54 nm in the channel containing the 12 MR supercages) with respect to ZSM-5 (0.53 nm × 0.56 nm in the straight channel running parallel to [0 1 0] and 0.51 nm × 0.55 nm in the sinusoidal channel running parallel to [1 0 0]) may favor the formation of benzene in detriment of the bulkier naphthalene product. On

* Corresponding author. Tel.: +34 963 877 808; fax: +34 963 877 809.
E-mail address: amart@itq.upv.es (A. Martínez).

0920-5861/$ – see front matter © 2005 Elsevier B.V. All rights reserved.
doi:10.1016/j.cattod.2005.07.051

the other hand, the better coke tolerance was ascribed to the presence of the large 12 MR cavities in MCM-22 acting as a trap for coke molecules.

Recently, a new material, called ITQ-2, has been prepared in our laboratories by delamination of the layered precursor of MCM-22 [8]. The delaminated zeolite is mostly formed by single layers organized in a ''house of card''-type structure having a very high external surface area. ITQ-2 consists of thin sheets 2.5 nm in height presenting a hexagonal array of ''cups'' (0.7 nm × 0.7 nm) that penetrate into the sheet from both sides connected by a double 6 MR window. These ''cups'' are the hemicavities related to the 12 MR supercages present in MCM-22 and which act as a coke trap during the MDA reaction. The sheets contain the 10 MR sinusoidal channel system of 0.40 nm × 0.59 nm size that is also present in MCM-22 and which is apparently responsible for the high selectivity of benzene displayed by Mo/HMCM-22 catalysts.

In view of this, in this work we have studied the possibilities of using the delaminated ITQ-2 zeolite as the acidic component of Mo-based MDA catalysts. The influence of the zeolite Si/Al ratio and of the surface dealumination on the activity and selectivity will be addressed. The catalytic properties of Mo/ITQ-2 will be compared with those of Mo/MCM-22 with the same Si/Al ratio. A thorough Molecular Dynamics simulation study of the diffusion of naphthalene at the MDA reaction temperature (973 K) in the two independent pore systems of MCM-22 has also been carried out. The results obtained allow accounting for the differences in selectivity found between the ITQ-2 and MCM-22 zeolites, as well as for the effects of the selective dealumination of the ITQ-2 external surface on product selectivity.

2. Experimental

2.1. Preparation of catalysts

The layered precursor of MCM-22, denoted as MCM-22(P), was synthesized using hexamethylenimine (HMI), silica (Aerosil 200, Degussa), sodium aluminate (56% Al_2O_3, 37% Na_2O, Carlo Erba), sodium hydroxide (98%, Prolabo) and deionized water, following the procedure reported in [8]. Thus, a gel of the following molar composition:

SiO_2:$x$$Al_2O_3$:0.10OH:0.18 Na:44.9 H_2O:0.50HMI

was prepared and crystallized in Teflon-lined stainless steel autoclaves at 423 K for 9 days. The concentration of Al in the synthesis gel was varied to obtain samples with Si/Al ratios of 15, 25, and 50. After crystallization, the solids were washed with deionized water and dried at 373 K to produce the layered precursor MCM-22(P). Then, the MCM-22(P) was swelled by mixing the solid with an aqueous solution of hexadecyltrimethylammonium bromide (CTABr) and an aqueous solution of tetrapropylammonium hydroxide (TPAOH, 40 wt.%), and the resulting solution was refluxed for 16 h at 353 K. The layers were forced apart by placing the slurry in an ultrasound bath (50 W, 40 kHz) for 1 h. Separation of the solids was done by acidification with concentrated hydrochloric acid (HCl, 37%) until the pH was below 2, followed by centrifugation. Calcination of the materials at 813 K yielded the ITQ-2 samples with different Si/Al ratios. These samples were denoted as I2-y, where y is the Si/Al ratio in the synthesis gel. A MCM-22 sample with Si/Al ratio of 15 was also prepared by calcination of the layered MCM-22(P) precursor (Si/Al = 15) at 853 K for 3 h. This sample was denoted as M22-15.

The calcined ITQ-2 sample with Si/Al ratio of 15 was submitted to a surface dealumination process with a 1.5 M aqueous solution of oxalic acid (99%, Fluka) at reflux and 343 K during 1.5 h using a liquid/solid ratio of 12 cm^3/g. After cooling at room temperature, the solid was filtered, extensively washed with deionized water, dried at 373 K, and finally calcined in a muffle at 773 K for 6 h. The acid-treated sample was denoted as I2-15-ox.

Molybdenum-containing catalysts were prepared by incipient wetness impregnation of the zeolite supports with an aqueous solution of ammonium heptamolybdate (Merck) to obtain a concentration of Mo in the final catalysts of 3 wt.%. After impregnation the materials were dried at 373 K and then calcined in a muffle oven at 773 K for 6 h.

2.2. Characterization of the materials

Powder X-ray diffraction was performed in a Philips X'pert diffractometer using monochromatized Cu Kα radiation to verify the quality of the synthesized zeolites. Textural properties of the zeolites and Mo-containing catalysts were obtained from the nitrogen adsorption isotherms measured at 77 K in a Micromeritics ASAP 2000 equipment. Surface areas were calculated by the BET method; micropore area and micropore volume were derived from the corresponding t-plots. External surface areas were then obtained by difference between the BET values and the micropore areas. Prior to the adsorption measurements the samples were degassed at 673 K and vacuum overnight.

X-ray photoelectron spectra (XPS) were acquired in a VG-Escalab-210 spectrometer using the Mg Kα radiation (1253.6 eV) operated at 20 mA, 10 kV, and a pass energy of the analyzer of 50 eV. The binding energy (BE) data were referenced to C 1s (284.5 eV). ^{27}Al solid-state nuclear magnetic resonance (NMR) spectra were recorded at room temperature in a Bruker AV400 spectrometer working at 104.2 MHz, using a 4 mm Bruker BL4 probe. Samples were packed into zirconia rotors and spun at the magic angle spinning (MAS) at rates of ca. 12 kHz. The ^{27}Al spectra were acquired with pulses of 0.5 μs corresponding to a flip angle of $\pi/20$ and were referred to a 0.1 M aqueous solution of $Al(NO_3)_3$.

The acidity of the samples was measured by infrared spectroscopy with adsorption–desorption of pyridine in a Nicolet 710 FTIR apparatus as detailed in [9]. The density of Brønsted and Lewis acid sites was determined from the intensities of the bands at about 1545 and 1450 cm^{-1}, respectively, using the molar extinction coefficients reported by Emeis [10]. The values obtained were referred to the acidity of the ITQ-2 sample with Si/Al ratio of 15, considering the number of Brønsted acid sites obtained at a desorption temperature of 523 K as 100.

Periodic atomistic molecular dynamics (MD) calculations were performed to simulate the diffusion of naphthalene in the purely siliceous MCM-22 structure [11], called ITQ-1, at the temperature used in the methane dehydroaromatization experiments (973 K). The zeolitic system comprises a $2 \times 2 \times 2$ macrocell of SiO_2 composition with a total of 1728 atoms to which periodic boundary conditions are applied. Runs of 400 ps, with a timestep of 1 fs, were carried out within NVE microcanonical ensemble. The loading simulated was 11 molecules of naphthalene in the ITQ-1 macrocell, with 9 molecules located in the supercages and 2 molecules located in the sinusoidal system. In all the simulations, every atom was allowed to move explicitly.

The MD simulations were carried out using the general purpose DL_POLY_2.11 code [12]. The expression used to calculate the diffusion coefficient, D, from the mean square displacements, was the following [13]:

$$\langle X^2(t) \rangle = 6 \cdot D \cdot t + B, \quad (1)$$

where 't' is the simulation time, and B is the thermal factor arising from atomic vibrations.

The trajectories followed by the hydrocarbons in their diffusion path through the MCM-22 structure are visualized by means of 'xy' and 'xz' projections, which highlight the motion in the 10 MR sinusoidal channels and 12 MR supercage systems. In order to facilitate the visualization, the channel structure is superimposed over the trajectories of the center of mass of each naphthalene molecule, and trajectories to each molecule are shown in a different gray fashion.

Four types of interatomic potentials are used to model this system:

$$V_{\text{total}} = V_{\text{zeolite}} + V_{\text{hydrocarbon}} + V_{\text{hc-hc}} + V_{\text{zeolite-hc}} \quad (2)$$

The potential for the framework, V_{zeolite}, was originally derived by Catlow et al. [14], whereas the potential for the sorbates, $V_{\text{hydrocarbon}}$, was taken from Oie et al. [15] and comprises two (bond), three (angle), and four-body (dihedral) interactions together with Coulomb terms. Two different atom types are considered in naphthalene, C and H, and the atomic charges for tertiary and quaternary carbons were −0.1190 and −0.0704, respectively, whereas the charge on hydrogen was 0.1014. More details of the potential parameters [16] and the techniques employed can be found in previous studies [17].

2.3. Catalytic experiments

The methane dehydroaromatization (MDA) experiments were carried out in a continuous down-flow fixed bed reactor at 973 K and atmospheric pressure. Typically, 0.4 g of catalyst previously crushed and sieved to a particle size of 0.25–0.42 mm were diluted with 2.0 g of silicon carbide (SiC) and loaded to the reactor. The catalysts were pretreated in situ by passing a flow of He (15 cm^3/min) through the bed from room temperature up to 973 K, and kept at this temperature for 30 min. Then, the He flow was stopped and a mixture of CH_4 and N_2 (used as internal standard) in a volumetric ratio of CH_4:N_2 = 9:1 was fed to the reactor at a flow rate of 10 cm^3/min, corresponding to a space velocity of 1500 $cm^3/(g_{cat}\ h)$.

The reaction products (including CO, C_2, and C_6–C_{10} aromatics) were separated and analyzed *on line* at different times on stream in a gas chromatograph (HP-GC6890) equipped with two columns (HayeSep Q and Molecular Sieve 5A) and two detectors (TCD and FID). Methane conversion and productivities were calculated on the basis of N_2 used as an internal standard. Yields and selectivities to the different products are given on a carbon basis.

In order to calculate the amount of carbonaceous deposits from the *on line* GC analyses, the mass flow rates of each carbon-containing species (unconverted methane, CO, C_2, C_6–C_{10} aromatics) at the reactor outlet were obtained from the corresponding GC peak areas and sensitivity factors in reference to that of N_2 (which remains unvaried during the reaction) and using methane as the link compound between TCD and FID analyses. Then, the carbon missing in the mass carbon balance is the carbon associated to carbonaceous deposits, which includes coke and heavy hydrocarbons that remained entrapped in the catalyst pores.

3. Results and discussion

3.1. Physico-chemical properties of the zeolites and Mo/zeolite catalysts

The X-ray diffraction (XRD) patterns of calcined ITQ-2 samples are shown in Fig. 1. As observed, the ITQ-2 sample with the highest Si/Al ratio (Si/Al = 50) does not show the 0 0 l peaks with the 2.5 nm periodicity typical of the MCM-22 structure (not shown), indicating a reduction of long-range order along the c axis, in agreement with the ITQ-2 structure in where the material is mostly formed by single layers. The intensity of the diffraction peaks increased with decreasing the Si/Al ratio, indicating that a lower degree of delamination was achieved at higher Al contents.

The chemical composition and textural properties of the calcined ITQ-2 and MCM-22 samples are given in Table 1.

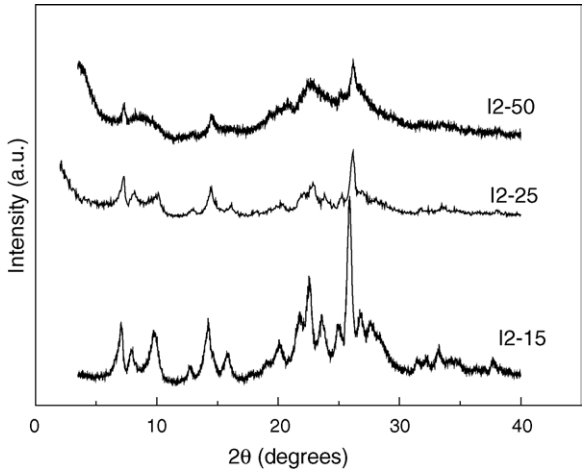

Fig. 1. X-ray diffraction patterns of calcined ITQ-2 samples with different Si/Al ratios.

As observed, the Si/Al ratios in the calcined materials practically matched the Si/Al ratios in the synthesis gels, indicating a complete incorporation of Al in the solids. The BET surface area and micropore volume of MCM-22 were 451 m^2/g and 0.16 cm^3/g, which are in close agreement with those previously reported [7,18]. It is seen that all ITQ-2 samples showed a higher BET surface area than MCM-22, which is mostly due to the contribution of the larger external surface area in the former. Moreover, as observed in Table 1 the external surface area increased significantly with decreasing the Al concentration, that is, with increasing the Si/Al ratio. This is in agreement with the XRD data presented above that showed a higher degree of delamination for the more siliceous ITQ-2 samples. However, it is clearly seen that the ITQ-2 sample with the lowest Si/Al ratio (I2-15) still presented a higher external surface area than that of MCM-22. A decrease of the surface area and pore volume was noticed in all samples after the incorporation of molybdenum, as shown in Table 2.

The relative acidity of the zeolites as determined by infrared spectroscopy with adsorption–desorption of pyridine is given in Table 3. As expected, the concentration of Brønsted acid sites for ITQ-2 samples decreased with increasing the Si/Al ratio. Treatment of the I2-15 sample with oxalic acid produced a significant reduction of the Brønsted acidity, which is attributed to the elimination of tetrahedral Al sites from the external surface, as this molecule cannot penetrate into the 10 MR pore system of the zeolite. In fact, the surface Si/Al ratio determined by XPS was seen to increase from 14 for the untreated I2-15 sample to 28 for the I2-15-ox sample. It is also seen in Table 3 that the number of Brønsted acid sites was higher for MCM-22 as compared with ITQ-2 with similar Si/Al ratio, which is attributed to a certain dealumination of the material during the delamination process.

Table 1
Chemical composition and textural properties of ITQ-2 and MCM-22 zeolites

Sample	Si/Al ratio	S_{BET} (m^2/g)	S_{ext} (m^2/g)	PV_{total} (cm^3/g)	V_{micro} (cm^3/g)
I2-15	14	520	217	0.33	0.13
I2-25	24	562	430	0.47	0.08
I2-50	46	895	835	0.99	0.04
M22-15	15	451	141	0.31	0.16

Table 2
Textural properties of Mo-containing catalysts as determined by N_2 adsorption

Sample	S_{BET} (m^2/g)	S_{ext} (m^2/g)	PV_{total} (cm^3/g)	V_{micro} (cm^3/g)
Mo/I2-15	434	195	0.72	0.12
Mo/I2-25	486	244	0.65	0.06
Mo/I2-50	743	689	0.94	0.02
Mo/I2-15-ox	513	278	0.70	0.11
Mo/M22-15	400	129	0.65	0.13

The effect of surface dealumination by acid treatment and Mo impregnation on the nature of the Al species present in ITQ-2 (Si/Al = 15) was studied by ^{27}Al MAS NMR. The spectra of the untreated and acid-treated ITQ-2 samples before and after Mo impregnation are presented in Fig. 2. The spectrum of the untreated I2-15 sample showed the peak at about 55 ppm, which is associated to four-coordinated framework Al species, and the peak at about 0 ppm of six-coordinated Al species in extraframework positions. After impregnation of 3 wt.% Mo, the peak intensity of the framework Al decreased while its line width at half height broadened. At the same time, the peak of extraframework Al at ca. 0 ppm also broadened and two new peaks appeared at about 14 and −13 ppm. The peak at ca. −13 ppm has been attributed to octahedral Al in $Al_2(MoO_4)_3$ species [19,20]. Moreover, the increase in the line width of the tetrahedral Al peak can be explained by a strong electrical field gradient at the nucleus caused by the presence of Mo [21], and suggests that Mo species are closely associated with framework Al. On the other hand, the signal at ca. 14 ppm has been attributed to octahedral Al in $MoO_3{\cdot}Al_2O_3{\cdot}nH_2O$ which is formed by hydrolysis of $Al_2(MoO_4)_3$ species [21]. Similar features have been observed in the ^{26}Al NMR spectrum of Mo/HZSM-5 [21].

As seen in Fig. 2, the intensity of the peaks at ca. 55 and 0 ppm of tetrahedral and octahedral Al species decreased after the treatment with oxalic acid, indicating that part of the Al present on the external surface of ITQ-2 was removed, in concurrence with the XPS data. Interestingly, the acid-

Table 3
Relative acidity (μmol Pyr/g) of ITQ-2 and MCM-22 zeolites as determined by infrared spectroscopy with adsorption–desorption of pyridine

Sample	Brønsted			Lewis		
	523 K	623 K	673 K	523 K	623 K	673 K
I2-15	100	69	23	63	54	50
I2-25	69	50	n.d.	31	32	n.d.
I2-50	25	13	n.d.	40	32	n.d.
I2-15-ox	58	37	13	25	25	21
M22-15	133	85	63	46	40	38

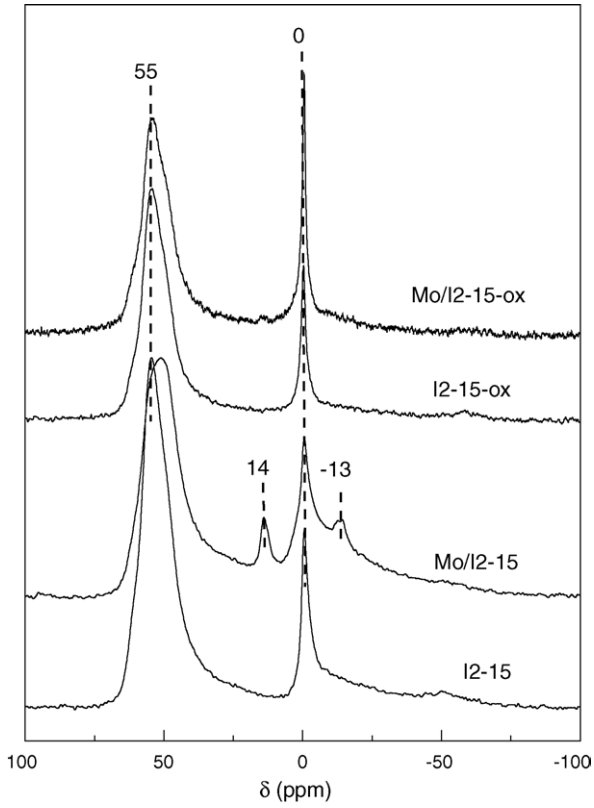

Fig. 2. ^{27}Al MAS NMR spectra of untreated and acid-treated ITQ-2 (Si/Al = 15) samples before and after Mo impregnation.

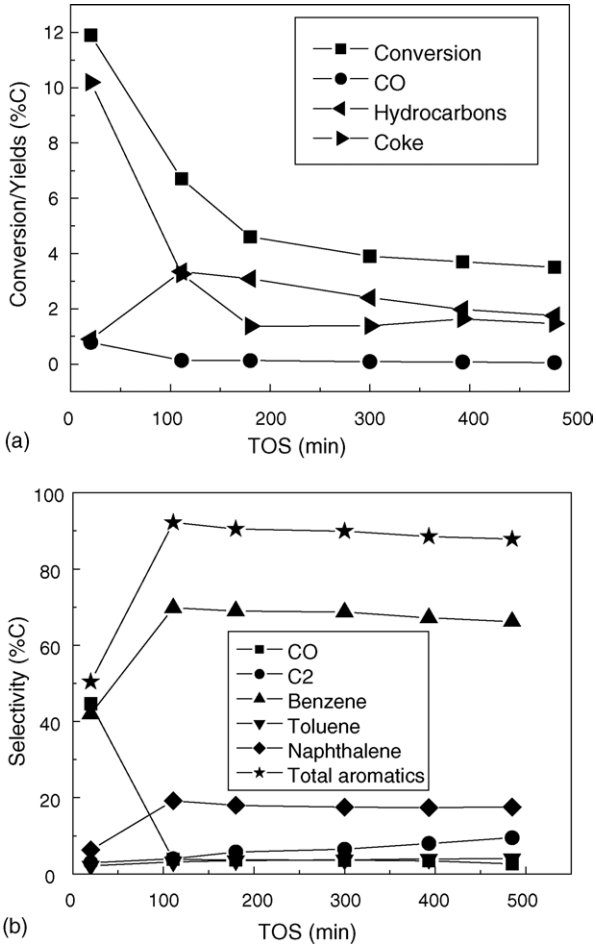

Fig. 3. Catalytic results for the MDA reaction over the Mo/I2-25 catalyst: (a) evolution of total methane conversion and product yields with TOS and (b) change of selectivity with TOS.

treated sample did not show the Al signals at ca. −13 and 14 ppm associated with the formation of $Al_2(MoO_4)_3$ species, suggesting that the concentration of framework Al on the surface of ITQ-2 after the dealumination treatment should be very small.

3.2. Catalytic results

3.2.1. Evolution of conversion and product yields/selectivities with TOS over Mo/ITQ-2

The non-oxidative conversion of methane at 973 K over Mo/ITQ-2 catalysts leads to the formation of the same type of products already observed in Mo/ZSM-5 and Mo/MCM-22. The main reaction products under the conditions used were coke, CO, and hydrocarbons (mainly ethane/ethylene, benzene, naphthalene, and toluene). The evolution of methane conversion and yields to the main reaction products with time on stream (TOS) for the Mo/I2-25 catalyst is displayed in Fig. 3a. At very short TOS, the total methane conversion amounted to about 12%, which is close to the values reported for Mo/HZSM-5 and Mo/HMCM-22 catalysts under similar reaction conditions [4,7]. At this stage of the reaction, a very large amount of coke was produced, with a yield of about 10% C. Both the methane conversion and coke yield rapidly decreased with TOS while the yield to hydrocarbons increased, reached a maximum at about 100 min TOS and then decreased slowly at larger TOS. It is seen that above 100 min TOS the yield to hydrocarbons (mainly aromatics) surpassed that of coke. Initially, a relatively high amount of CO was produced, which then decreased and remained almost constant for TOS above ca. 100 min. The formation of high amounts of CO (and CO_2) during the initial reaction stages (induction period) is explained by the removal of oxygen from the MoO_x precursors by reaction with the methane feed at the MDA reaction temperatures [22–27]. This leads to the gradual reduction of Mo oxide species into Mo_2C and/or MoO_xC_y species, which are presumably the active phases for the activation of methane.

The change of selectivity to the main reaction products (excluding carbonaceous deposits) with TOS for the Mo/I2-25 catalyst is presented in Fig. 3b. At short TOS (20 min) CO was the main reaction product with a selectivity of ca. 45%, followed by benzene (ca. 42% selectivity). At this stage the selectivity to naphthalene, toluene, and C_2 hydrocarbons (mainly ethylene) were rather low. The CO selectivity drastically dropped with TOS reaching a value of less than 4% at TOS above ca. 100 min. At the same time, the

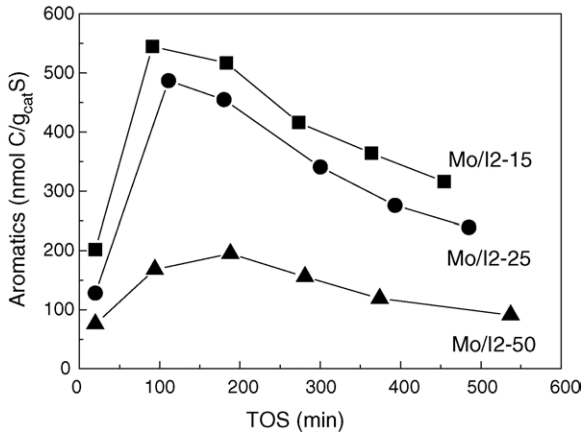

Fig. 4. Rate of aromatics formation for Mo/ITQ-2 catalysts, as a function of TOS.

selectivity to benzene and naphthalene sharply increased up to a TOS of ca. 100 min, and then slightly decreased at larger TOS. Maximum selectivities to benzene and naphthalene of ca. 70 and 20%, respectively, were obtained over the Mo/I2-25 catalyst. The selectivity to toluene, which was formed in very low amounts, increased very slowly with TOS, while that of C_2 attained a value of ca. 10% after about 6 h on stream.

3.2.2. Influence of the Si/Al ratio in Mo/ITQ-2 catalysts and comparison with Mo/MCM-22

All the Mo/ITQ-2 and Mo/MCM-22 samples studied showed the same catalytic behavior during the MDA reaction discussed above for the Mo/I2-25 sample. For simplicity and clarity, the discussion on the influence of the Si/Al ratio in Mo/ITQ-2 and the comparison with Mo/MCM-22 will be established on the basis of product yields/selectivities excluding the carbonaceous deposits. First, the influence of Si/Al ratio in ITQ-2 on the rate of aromatics formation is presented in Fig. 4. As observed, the rate increases initially for all catalysts, reaches a maximum at about 90–180 min on stream depending on the Si/Al ratio, and then decreases at larger TOS. The initial increase corresponds to the induction period commented before. As observed in Fig. 4, the rate of aromatics formation increases when decreasing the Si/Al ratio of the ITQ-2 zeolite, that is, when increasing the density of Brønsted acid sites. A close relationship between the Brønsted acidity and rate of aromatics formation was also observed in the case of Mo/HZSM-5 catalysts [28].

The selectivities to the different reaction products at the maximum aromatics formation are given in Table 4. The selectivity to CO and C_2 raised with increasing the Si/Al ratio of the ITQ-2 zeolite. This result indicate a decrease in the aromatization rate of the intermediate C2 species when decreasing the amount of Brønsted acid sites in ITQ-2, and clearly suggests a direct participation of the acid sites in the final aromatization step. On the other hand, the selectivity to naphthalene decreases when increasing the Si/Al ratio. In all cases, the selectivity to benzene was fairly larger than that of naphthalene, despite the later being thermodynamically more stable, indicating that benzene is kinetically favored. We may speculate at this point that the formation of naphthalene should take place preferentially on the acid sites located on the external surface of ITQ-2. If this is so, then the formation of naphthalene should be favored on the ITQ-2 sample presenting the largest amount of Brønsted acid sites accessible through the external surface area, as it is experimentally observed. We will come back to this point later when discussing the results of the molecular dynamics simulation study. As a result of the opposite trends observed for CO and C_2 on one hand and naphthalene on the other when varying the Si/Al ratio, a maximum selectivity to benzene of about 70% was found for the catalyst prepared from the ITQ-2 sample with intermediate Si/Al ratio (Mo/I2-25).

The results obtained for the Mo/M22-15 catalyst are also included in Table 4. At the maximum of activity, Mo/M22-15 shows a higher methane conversion than the Mo/ITQ-2 sample with similar Si/Al ratio (Mo/I2-15), in agreement with the higher Brønsted acidity of the MCM-22 zeolite (Table 3). Moreover, at maximum activity MCM-22 shows a slightly higher selectivity to benzene and lower to naphthalene than ITQ-2. These differences were even higher at larger TOS since the increment in selectivity to naphthalene is larger for Mo/ITQ-2 than for Mo/MCM-22 (Fig. 5). These results might be well explained by considering the structural differences between these two zeolites and by assuming that benzene is preferentially formed inside the circular 10 MR channels present in both structures, while the formation of naphthalene occurs predominantly on the external zeolite surface, as will be shown later by the theoretical study.

Table 4
Comparison of product selectivities (excluding coke) at the maximum of aromatics formation for Mo/ITQ-2 and Mo/MCM-22 catalysts

Catalyst	TOS (min)	CH_4 conversion (%)	Selectivity (% C)				
			CO	C_2	Benzene	Toluene	Naphthalene
Mo/I2-15	91	3.8	3.1	3.5	62.2	3.1	28.1
Mo/I2-25	111	3.5	3.8	4.0	69.8	3.2	19.2
Mo/I2-50	188	1.5	8.6	7.7	66.2	3.4	14.1
Mo/M22-15	92	4.8	3.8	3.4	64.8	3.2	24.8

Reaction conditions: 973 K, space velocity = 1500 $cm^3/(g_{cat}\ h)$, CH_4/N_2 vol. ratio = 9/1.

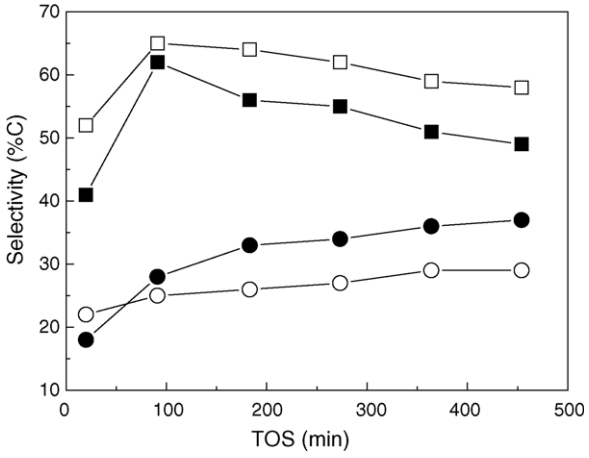

Fig. 5. Selectivity to benzene (squares) and naphthalene (circles) as a function of TOS for the Mo/I2-15 (solid symbols) and Mo/M22-15 (open symbols) catalysts.

3.2.3. *Influence of the selective surface dealumination of ITQ-2*

In order to improve the selectivity to benzene and to reduce the formation of naphthalene in the case of Mo/ITQ-2, we have carried out the selective dealumination of the external surface of ITQ-2 (Si/Al = 15) by treating the zeolite with an aqueous solution of oxalic acid. This treatment slightly decreases the maximum rate of aromatics formation from 545 nmol C/(g_{cat} s) for the untreated sample to 422 nmol C/(g_{cat} s) for the acid-treated Mo/I2-15-ox catalyst. Such a decrease is well explained by the decrease in the Brønsted acidity of the zeolite observed after the acid treatment (Table 3). However, the acid treatment produces a significant improvement in the selectivity to benzene in detriment of naphthalene (Fig. 6). Thus, at the maximum of activity (TOS = 90–100 min) the benzene selectivity increases from ca. 62 up to 75% while that of naphthalene is drastically reduced from ca. 28 to 14%. It is worth noting

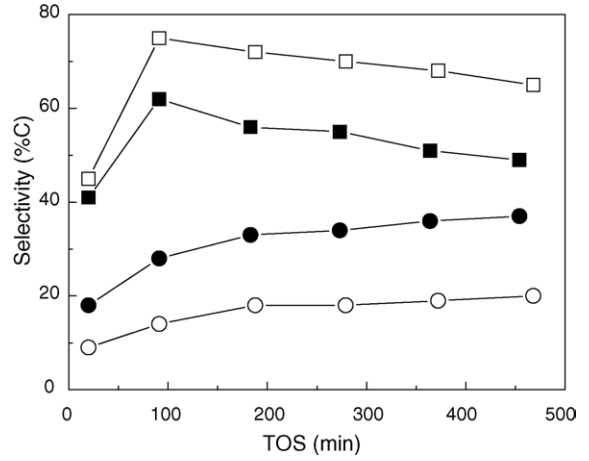

Fig. 6. Selectivity to benzene (squares) and naphthalene (circles) as a function of TOS for the Mo/I2-15 (solid symbols) and the acid-treated Mo/I2-15-ox (open symbols) catalysts.

that the maximum benzene selectivity achieved over the acid-treated Mo/ITQ-2 catalyst is significantly higher than that obtained over Mo/MCM-22 (ca. 65%) under the same reaction conditions. These results can be explained by the selective removal of Al from the zeolite surface after the acid treatment, as deduced from the XPS data, which results in a decreased concentration of Brønsted acid sites on the external surface of the ITQ-2 layers where, presumably, the thermodynamically favored naphthalene molecules are preferentially formed in the absence of shape selectivity effects.

In order to better explain the differences in selectivity between ITQ-2 and MCM-22 and the effect of surface dealumination, we have carried out a molecular dynamics simulation study of the diffusion of naphthalene in the two independent pore systems of MCM-22. It has to be noted that the sinusoidal 10 MR pore system is common to both catalysts while the pore system containing the supercages delimited by 12 MR but accessed only through 10 MR windows is characteristic for MCM-22 but not for ITQ-2 with a high degree of delamination. Even considering that a complete delamination is not achieved for ITQ-2 samples with low Si/Al ratios, the number of supercages will be always higher for MCM-22.

3.3. *Molecular dynamics simulation study of naphthalene in MCM-22*

First, the trajectories of naphthalene in the 10 MR sinusoidal channels of MCM-22 were studied. Molecules labeled ‘10’ and ‘11’ (Fig. 7a) diffused through the 10 MR sinusoidal system and it is seen that in spite of the small size of the channel section, the naphthalene molecules diffused through this channel system. This result was surprising, since in a previous study using the same methodology [29] it was shown that benzene does not diffuse through the 10 MR sinusoidal system of MCM-22 at 650 K. Instead, the benzene molecules were found to remain at locations near the minimum energy position in this system. In this case, the larger temperature of the simulations used here (973 K) explain the results found. Small activation energies for diffusion may be overcame by temperature activation and in the present case, the 323 K larger reaction temperature of this study seems to be the key factor to explain why a large molecule such as naphthalene diffuses through the narrow and sinusoidal medium pore channel in MCM-22. It is also clear from our results that the tortuosity of the 10 MR channels will be responsible for a larger diffusivity of benzene with respect to naphthalene at a given temperature. Also, in spite of the diffusivity observed in Fig. 7a, it can be seen that for long times, the molecules ‘10’ and ‘11’ are staying in locations near the minimum energy positions. Those minima in the 10 MR system were located in the middle of the hexagonal features as in the marked as ‘m10’ (Fig. 7a), whereas the path in between are locations where the potential energy raises and this makes that naphthalene

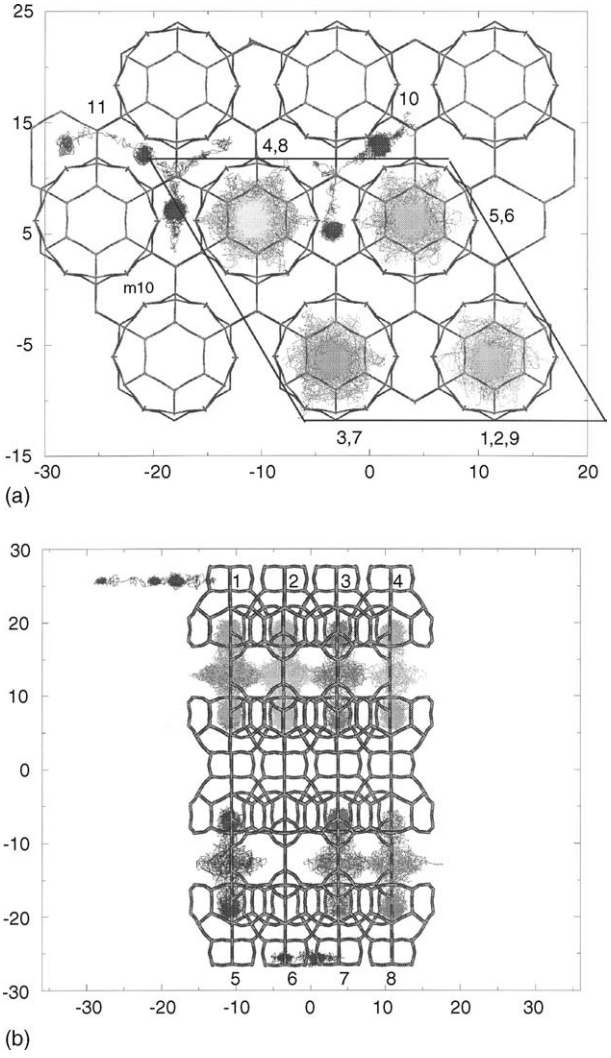

Fig. 7. (a) Trajectories of the 11 naphthalene molecules in MCM-22 at 973 K. The axes shown are '*y*' and '*x*' for the vertical and horizontal, respectively. Molecules labelled 1–9 are diffusing through the supercavities and it is seen that no intercage migration is shown. Molecules 10 and 11 are diffusing through the 10 MR channel system. (b) Trajectories of the naphthalene molecules in MCM-22 at 973 K. The vertical and horizontal axes are '*z*' and '*x*', respectively. Supercavities are labelled 1–8, and the molecular occupations in cavities are as follows: molecules 1, 2 are in cavity 1; 5, 6 in cavity 2; 3 in cavity 3; 4 in cavity 4; 9 in cavity 5; 7 in cavity 7; 8 in cavity 8. Molecules 10, 11 diffuse through the 10 MR channels (better viewed in (a)).

molecules to spent considerably less time. From the molecular dynamics runs, the mean square displacements were obtained and the corresponding diffusion coefficient for the diffusion of naphthalene in the sinusoidal 10 MR channels of MCM-22 (and ITQ-2) at 973 K was calculated as 2.2×10^{-6} cm^2/s.

The trajectories of naphthalene in the pore system containing the supercages can be observed from Fig. 7a and b. The '*yx*' projection in Fig. 7a is very appropriate to see intercage motions, which would be perpendicular to the supercage axis and no intercage diffusion was seen in spite of the high temperature. A previous study with benzene [29] showed no intercage motions at 650 K, and a few intercage events at 850 K. It was shown that the main difficulty for the intercage migrations was not the size of the connecting 10 MR windows between cavities but rather the fact that the intracage and intercage diffusivities occur perpendicularly and a quick change of 90° in the diffusion velocity vector at the 10 MR heights is not a probable option. The same can be said in the case of naphthalene, for which the orientational change should be more difficult than for benzene due to the larger size of the former, resulting in negligible intercage diffusion. Fig. 7b allows appreciating the intracage motions of the naphthalene molecules. In cavities with one molecule, jumps were observed between the two minima present in the supercages, which are located at opposite sides, with no apparent activation energy. In cases where cavities were occupied by two molecules (see, for example, cavity 1 in Fig. 7b) it was seen that both molecules occupied the whole cavity, which means that they jump and both molecules can be, during certain time, in the same part of the supercage. A high loading of molecules may be possible although in a MCM-22 crystal, once the supercages in the surface are filled, the diffusion through the crystal will be limited by the intercage motions and this will pose a high impediment for diffusion of naphthalene through the supercages. A much larger diffusion may be expected in ITQ-2, where the supercages can be accessed from the surface without the need to diffuse through the connecting 10 MR windows between supercages.

The above MD results clearly revealed that naphthalene is preferentially formed on the external surface of the zeolites studied, and thus, a higher selectivity to this product can be expected for the delaminated Mo/ITQ-2 catalysts as compared with Mo/MCM-22, as it is experimentally observed. Moreover, they allowed explaining the drastic drop in naphthalene selectivity observed after the selective dealumination of the external surface of ITQ-2.

4. Conclusions

Bifunctional Mo/ITQ-2 catalysts (3 wt.% Mo) have been used for the methane dehydroaromatization (MDA) reaction under non-oxidative conditions at 973 K and atmospheric pressure. The activity and selectivity of Mo/ITQ-2 catalysts were affected by the Si/Al ratio of the zeolite, that is, by the density of Brønsted acid sites. The rate of aromatics formation and the selectivity to naphthalene increased with decreasing the Si/Al ratio, while a maximum selectivity to benzene (ca. 70%) was found for the zeolite with intermediate Si/Al ratio (25). When compared with a MCM-22 zeolite with the same chemical composition (Si/Al = 15) the catalyst based on ITQ-2 produced more naphthalene and less benzene. The selectivity to benzene was significantly improved by submitting the ITQ-2 zeolite to a surface dealumination treatment with oxalic acid, which drastically reduced the formation of naphthalene on the

external surface of the zeolite. At the maximum of activity, the benzene selectivity for the acid-treated zeolite reached a value of ca. 75%, which was significantly higher than the maximum selectivity attained over Mo/MCM-22 (ca. 65%). The higher selectivity to naphthalene of the untreated ITQ-2 catalyst as compared to MCM-22 and the decreased formation of naphthalene after the selective surface dealumination treatment suggest that this product is predominantly formed on the highly accessible acid sites at the external surface of ITQ-2, as further supported by molecular dynamics simulation.

Acknowledgments

Financial support by the Comisión Interministerial de Ciencia y Tecnología (CICYT) of Spain through the projects MAT2001-2726 and MAT2003-07769-C02-01 is gratefully acknowledged. E.P. thanks the Ministerio de Ciencia y Tecnología for a Ph.D. scholarship. We also thank CIEMAT (Centro de Investigaciones Energéticas, Medioambientales y Tecnológicas) for the use of their computational facilities.

References

[1] J.H. Lunsford, Catal. Today 63 (2000) 165.
[2] L. Wang, L. Tao, M. Xie, G. Xu, J. Huang, Y. Xu, Catal. Lett. 21 (1993) 35.
[3] Y. Xu, L. Lin, Appl. Catal. A 188 (1999) 53.
[4] Y. Shu, M. Ichikawa, Catal. Today 71 (2001) 55.
[5] C. Zhang, S. Li, Y. Yuan, W. Zhang, T. Wu, L. Lin, Catal. Lett. 56 (1998) 207.
[6] D. Ma, Y. Shu, M. Cheng, Y. Xu, X. Bao, J. Catal. 194 (2000) 105.
[7] Y. Shu, D. Ma, L. Xu, Y. Xu, X. Bao, Catal. Lett. 70 (2000) 67.
[8] A. Corma, V. Fornés, S.B. Pergher, Th.L.M. Maesen, J.G. Buglas, Nature 396 (1998) 353.
[9] A. Corma, V. Fornés, A. Martínez, J. Sanz, ACS Symp. Ser. 375 (1988) 17.
[10] C.A. Emeis, J. Catal. 141 (1993) 347.
[11] M.A. Camblor, C. Corell, A. Corma, M.J. Diaz-Cabañas, S. Nicopoulos, J.M. Gonzalez-Calbet, M. Vallet-Regi, Chem. Mater. 8 (1996) 2415.
[12] W. Smith, T.R. Forester, J. Molec. Graphics 14 (1996) 136.
[13] M.P. Allen, D. Tildesley, Molecular Simulation of Liquids, Oxford University Press, 1980.
[14] C.R.A. Catlow, C.M. Freeman, B. Vessal, S.M. Tomlinson, M.J. Leslie, J. Chem. Soc. Faraday Trans. 87 (1991) 1947.
[15] T. Oie, T.M. Maggiora, R.E. Christoffersen, D.J. Duchamp, Int. J. Quantum Chem., Quantum Biol. Symp. 8 (1981) 1.
[16] G. Sastre, N. Raj, C.R.A. Catlow, R. Roque-Malherbe, A. Corma, J. Phys. Chem. B 102 (1998) 3198.
[17] A. Corma, C.R.A. Catlow, G. Sastre, J. Phys. Chem. B 102 (1998) 7085.
[18] A. Corma, C. Corell, J. Pérez-Pariente, J.M. Guil, R. Guil-Lopez, S. Nicolopoulus, J. González-Calbet, M. Vallet-Regi, Zeolites 16 (1996) 7.
[19] W. Liu, Y. Xu, S. Wong, L. Wang, J. Qin, N. Yang, J. Mol. Catal. A 120 (1997) 257.
[20] J.Z. Zhang, M.A. Long, R.F. Howe, Catal. Today 44 (1998) 293.
[21] W. Zhang, D. Ma, X. Han, X. Liu, X. Bao, X. Guo, X. Wang, J. Catal. 188 (1999) 393.
[22] J.H. Lunsford, M.P. Rosynek, D. Wang, Stud. Surf. Sci. Catal. 107 (1997) 257.
[23] H. Jiang, L. Wang, W. Cui, Y. Xu, Catal. Lett. 57 (1999) 95.
[24] Y.-H. Kim, R.W. Borry III, E. Iglesia, Microporous Mesoporous Mater. 35–36 (2000) 495.
[25] W. Ding, S. Li, G.D. Meitzner, E. Iglesia, J. Phys. Chem. B 105 (2001) 506.
[26] F. Solymosi, A. Erdohelyi, A. Szoke, Catal. Lett. 32 (1995) 43.
[27] F. Solymosi, A. Szoke, J. Cserenyi, Appl. Catal. A 142 (1996) 361.
[28] S. Liu, L. Wang, R. Onishi, M. Ichikawa, J. Catal. 181 (1999) 175.
[29] G. Sastre, C.R.A. Catlow, A. Corma, J. Phys. Chem. B 103 (1999) 5187.